ORIGINAL RESEARCH (AR) DOI: 10.4274/jems.2025.26097

Journal of ETA Maritime Science

Performance Analysis of Interacting Rigid Wind Sails and Rotor Sails by Kriging Surrogate Model

Takumi Endo[1], Cem Güzelbulut[2]

[1]The University of Tokyo Graduate School of Engineering, Department of Mechanical Engineering, Tokyo, Japan
[2]Kahramanmaraş İstiklal University, Department of Mechanical Engineering, Kahramanmaraş, Türkiye

Abstract

Increasing global CO_2 emissions lead to all industries, including the maritime industry, to adopt environmentally friendly solutions. Using wind energy, introducing alternative fuels, building carbon capture and storage systems, and improving the operation by route optimization and voyage speed control are some of the attempts to achieve this. In the present study, an investigation of the efficiency of implementing one rigid wind sail and one rotor sail was conducted to optimize the use of both systems to their maximum potential. A case study was designed to understand how much interaction between sails plays a role and how to use multiple sailing systems considering the interaction model. A kriging surrogate model was created to model the interaction between sails, and the maximum prediction error was found to be 8% in the lift coefficient prediction of the rotor sail. Then, the ship dynamics model, known as the Maneuvering Modeling Group model, was built. It was found that interaction significantly affects the performance of sails, approximately 4%, and using a surrogate model-based controller contributes around 1% more than that of an independent controller to the reduction of power required to maintain ship speed.

Keywords: Rigid wind sail, rotor sail, wind-assisted ship propulsion, kriging surrogate model

1. Introduction

The International Maritime Organization introduced regulations to deal with increasing CO_2 emissions and achieve net-zero emissions by 2050 in shipping [1]. Thus, many innovations and ideas are being produced to achieve net-zero emissions. Bouman et al. [2] listed decarbonization efforts in the maritime industry and categorized them into hull design, propulsion systems, alternative fuels, implementation of other energy sources, and operation-related improvements. Serra and Fancello [3] conducted a detailed review on alternative solutions to achieve decarbonizing shipping and provided advantages and disadvantages of each option. In the present study, wind-assisted ships that include different sailing systems, are being investigated to combine the benefits of each sailing system depending on wind direction, thus improving the total benefit that can be acquired.

Wind-assisted propulsion systems use sailing systems as auxiliary propulsors and reduce the required power by engine, thus contribute to fuel savings and reducing CO_2 emissions. The main types of wind-assisted ship propulsion systems are rigid wind sails, rotor sails, kites and suction sails. Rigid wind sails have an airfoil, which generates lift and drag forces due to pressure differences. By controlling the angle of attack (*AoA*), thrust force is maximized to assist the propulsion system and reduce the load on the engine, which leads to fuel savings. Since wind can come from any direction, symmetrical National Advisory Committee for Aeronautics (NACA) airfoils, multi-element wings and crescent-like airfoils were proposed to be used in wind sailing systems. Kramer and Steen [4] used NACA0015 airfoils and calculated fuel savings for different operational and design conditions. von Klemperer et al. [5] proposed an articulating sailing system based on NACA0020 airfoil and found that articulating airfoils can generate 30% larger lift forces compared to the fixed airfoil. Zhu et al. [6] proposed a crescent-like airfoil for rigid wind sails and compared it to a classical NACA0015 airfoil. It was found that crescent-like airfoils can generate larger thrust than classical NACA0015

Address for Correspondence: Asst. Prof. Cem Güzelbulut, Kahramanmaraş İstiklal University, Department of Mechanical Engineering, Kahramanmaraş, Türkiye
E-mail: cem.guzelbulut@istiklal.edu.tr
ORCID iD: orcid.org/0000-0001-9618-4032

Received: 03.06.2025
Last Revision Received: 15.08.2025
Accepted: 14.10.2025
Epub: 18.11.2025

To cite this article: T. Endo, and C. Güzelbulut, “Performance analysis of interacting rigid wind sails and rotor sails by kriging surrogate model,” *Journal of ETA Maritime Science*, [Epub Ahead of Print]

airfoils. Then, Guzelbulut et al. [7] proposed a parametric crescent airfoil and optimized the shape of the crescent airfoil. The optimal crescent airfoil improved the efficiency of the sailing systems up to 22% depending on the wind direction. Unlike rigid wind sails, rotor sails are active devices which require steady power input. Rotor sails are cylinder-like structures and generate lift and drag forces due to pressure difference caused by rotational movement along their vertical axis. Tillig and Ringsberg [8] investigated the effectiveness of different Flettner rotor arrangements using a 4-degree-of-freedom model. To understand how the design and operational parameters of a single rotor sail affect the aerodynamics, Kwon et al. [9] conducted 3D fluid dynamics simulations considering aspect ratio, diameter ratio, and spin ratio. Guzelbulut et al. [10] considered different control strategies for the sailing system and the ship dynamics of a ship equipped with four rotor sails and concluded that integrating the ship dynamics controller and the sail controller can lead to further fuel savings. Since wind speed at higher altitudes is significantly stronger, static and dynamic kites were proposed, to harness this increased wind potential. Goksu and Erginer [11] investigated the canopy curvature of a kite on aerodynamic characteristics and towing force for wind-assisted ships. Dadd et al. [12] conducted an optimization study to find the optimal design and the operation of a dynamic kite. In the present study, we examined whether using two different sailing systems together can have potential benefits or not.

When using multiple sailing systems together, interactions between sails play a significant role. Tillig and Ringsberg [8] used potential flow theory to determine the interaction between multiple rotor sails. [illegible] Vilanova et al. [13], applied Gaussian Process Regression and fully connected neural networks to model the interaction between three DynaRig configurations. Zhang et al. [14] examined the effect of desynchronous control of two interacting rigid wind sails having crescent-like airfoils using kriging surrogate models. [illegible] et al. [illegible] also implemented a kriging surrogate model to model the interaction behavior of three symmetrical NACA[illegible] airfoils. However, the interaction between different sailing systems and whether using different sailing systems together leads to synergistic improvement of the efficiency of the sailing systems still remain ambiguous. In the present study, we aimed to model the interaction between two different sail types using a surrogate model fitted by 3D fluid dynamics simulation.

In the present study, we first generated samples based on Latin Hypercube sampling (LHS) and conducted 3D computational fluid dynamics (CFD) simulations to create a database of aerodynamic and operational parameters. The interaction between sailing systems was estimated using an ordinary Kriging surrogate model. Finally, we conducted a case study to understand the effect of interactions between sailing systems. We examined how a controller, integrating an interaction surrogate model, can lead to further improvements to reduce propeller power.

2. Methodology

In the present study, we first conducted CFD simulations to understand how the aerodynamics of sails [illegible] depend[illegible] on the *AoA* of the rigid wind sails, spin ratio of rotor sails, and apparent wind direction. A kriging surrogate model was created following CFD simulations, whose conditions were determined by LHS, to understand the interaction between sailing systems. Finally, the interaction effect between sailing systems and the effect of synergistic control actions were investigated through the Maneuvering Modeling Group (MMG) model.

2.1. CFD Simulations

In the present study, CFD simulations were conducted to characterize the aerodynamics of interacting sails. The aerodynamic parameters of interest are the lift and drag coefficients for both sailing systems, c_L and c_D, and the power coefficient for rotor sails, c_P, which were defined as given in Equations 1-3, where L and D are the lift and drag forces, P is the power required to rotate the rotor sail, ρ_{air} is the density of air (1.225 kg/m^3), V_A is the apparent wind speed, and A is the projected area of the sails. The rotor sail used in the study has a diameter of 5 m and a height of 30 m, resulting in a projected area, A, of 150 m^2. When it comes to a rigid wind sail, it has a chord length of 14 m and height of 50 m and results in a projected area, A, of 700 m^2.

$$c_D = \frac{D}{\frac{1}{2}\rho_{air}V_A^2 A} \quad (1)$$

$$c_L = \frac{L}{\frac{1}{2}\rho_{air}V_A^2 A} \quad (2)$$

$$c_P = \frac{P}{\frac{1}{2}\rho_{air}V_A^3 A} \quad (3)$$

While the aerodynamics of rigid wind sails depends on *AoA*, that of rotor sail is characterized by spin ratio, which is the ratio of tangential speed to apparent wind speed, as given in Equation 4. ω and R are the angular speed and the radius of rotor sails, respectively. The radius of the rotor sail is 2.5 m.

$$SR = \frac{\omega R}{V_A} \quad (4)$$

The computational domain used in CFD simulations is three-dimensional having the following arrangement, positioning and boundary conditions:

- The distance between rotor sail and rigid wind sail is set to be 100 m
- The mid-point of sailing system is set to be 200 m away from the inlet
- ϑ defines the apparent wind direction
- The size of the computational domain is 600x300x100 m^3
- Inlet fluid speed is set to be 10 m/s
- Slip boundary condition was defined on bottom surface on xy plane
- Wall (no-slip) boundary conditions were defined on the outer surfaces of both sailing systems
- The remaining surfaces were set to be an outlet boundary conditions as shown in Figures 1 and 2.

CFD simulations were performed on Altair Hypermesh CFD 2023 and AcuSolve 2023 based on a steady-solution of the Reynolds-Averaged Navier-Stokes equations with Shear Stress Transport (SST) k-ω turbulent modeling. The properties of the fluid are given in Table 1.

The following mesh refinements around rotor sail and rigid wind sail were assigned to computational volume to capture the acting forces.

- The maximum length of edges around the rigid wind sail and rotor sail is 0.1 m.
- The number of prism elements around the rotor sail is [illegible], with a growth rate of 1.3. The thickness of the first edge layer around the rotor sails is 0.0001 m.
- The number of prism elements around the rigid wind sail is 10, with a growth rate of 1.3. The thickness of the first edge layer around the rotor sails is 0.005 m.
- The element size of surface elements on rigid wind sails and rotor sails is 0.3 m.
- The maximum global volume mesh size is [illegible] with a growth rate of 1.2.

2.2. Sampling of CFD Database

To establish a surrogate model of interacting sailing systems, a set of data is required. There are various methods for determining the sampling points to be simulated. LHS was chosen due to its extensive use in CFD applications and kriging surrogate models. Inputs of the surrogate model were the *AoA* of the rigid wind sail, the spin ratio of the rotor sail, and the apparent wind direction. Sampling points for each parameter are presented in Table 2.

Table 1. *Physical properties of [illegible]*

Property	Value
Density	1.225 kg/m^3
Dynamic viscosity	1.781x10^{-5} kg/ms

Table 2. *Sampling points for each input parameter*

Parameter (Unit)	Sampling points
Angle of attack (deg)	-90, -75, -50, -40, -30, -25, -20, -15, -10, -5, 0, 5, 10, 15, 20, 25, 30, 40, 50, 75, 90
Spin ratio (-)	-5, -3, -2, -1, 0 ,1, 2, 3, 5
Apparent wind direction (deg)	0, 30, 60, 90, 120, 150, 180

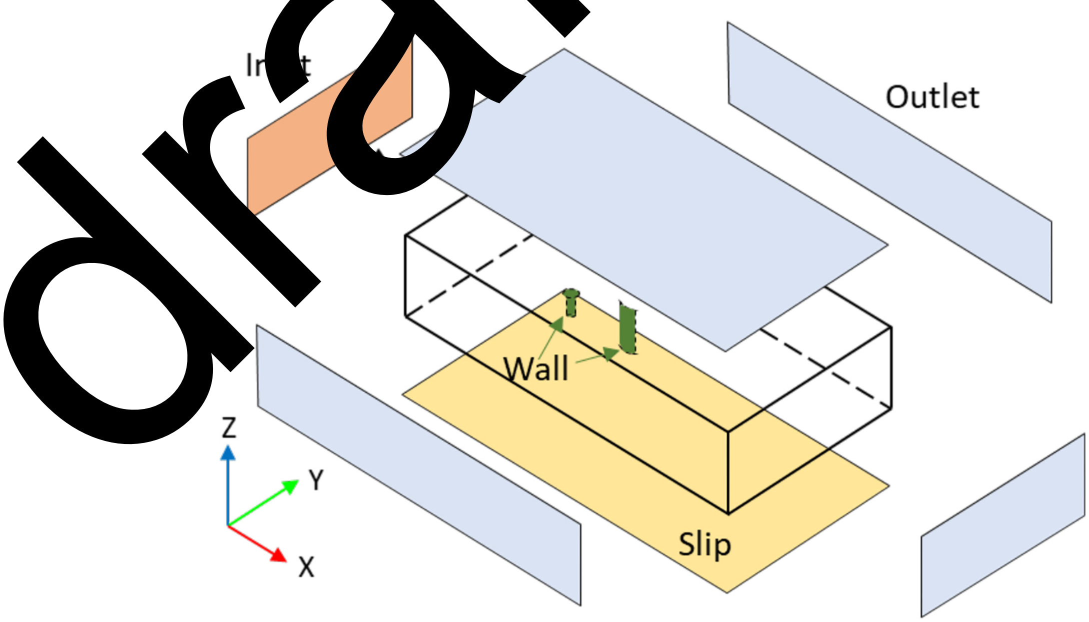

Figure 1. *Boundary conditions and computational volume of the problem*

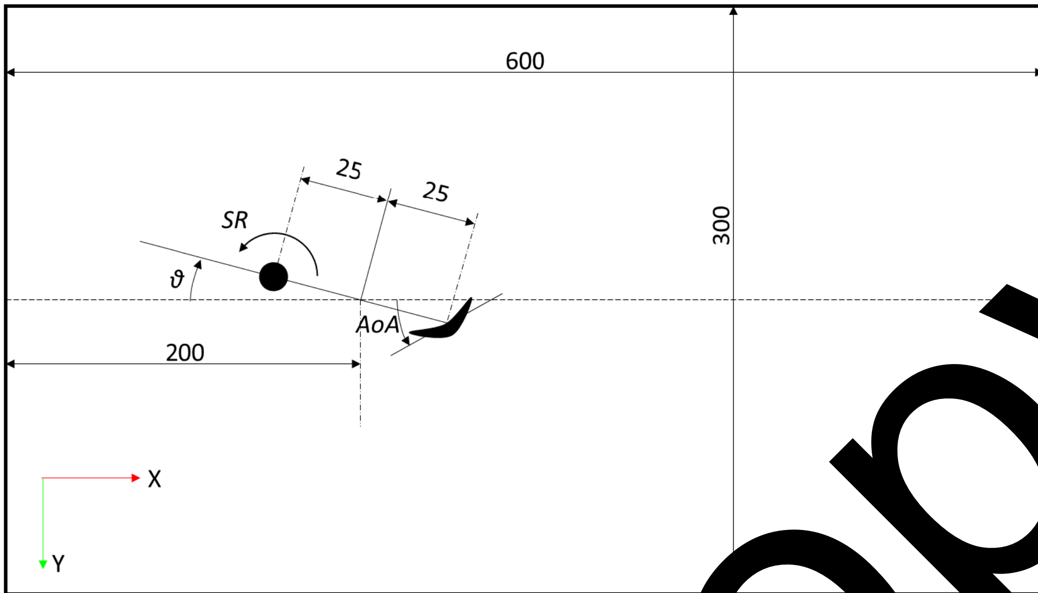

Figure 2. *The dimensions of computational volume and the definitions of the parameters used in CFD simulations*
CFD: Computational fluid dynamics, SR: Spin ratio, AoA: Angle of attack

The airfoil used in the present study is a crescent-like airfoil obtained by previous study conducted by Zhu et al. [6], and has a maximum lift around *AoA* of 20 deg. Therefore, data points were concentrated within the range of 10-30 degrees. When it comes to rotor sails, previous studies characterized the behavior of rotor sails for the spin ratio range of 0-5, which justifies the spin ratio range determined. The sign of the spin ratio implies whether the rotor sail rotates in a clockwise or counterclockwise direction.

LHS is a design of experiment technique that statistically reduces the total possible combinations of each design variable. More precisely, it uniformly distributes each sample point within the design space. Using LHS, 170 different conditions in which *AoA*, spin ratio and apparent wind direction were uniformly distributed across given sampling points were generated. Sampling points were divided into 85% training data points and 15% test data points.

2.3. Kriging Surrogate Model

Surrogate models are approximation methods to express complex behaviors and to reduce computational time. In the present study, we adopted an ordinary kriging surrogate model. Kriging surrogate models are interpolation-based surrogate models and approach the real function as given in Equation 5, where $\hat{y}$ is predicted response, and $Z(\boldsymbol{x})$ are mean and deviation terms, and $\boldsymbol{x}$ is the parameters vector. In ordinary kriging surrogate models, the mean term is a zero-order polynomial function.

$$\hat{y} = \hat{\mu} + Z(\boldsymbol{x}) \tag{5}$$

To establish an ordinary kriging surrogate model, covariance is defined to understand the proximity of the sampling points, as shown in Equation 6, where σ^2 is the variance, and $R(x^{(i)}, x^{(j)})$ is the correlation function. In the present study, the Gaussian correlation function, as given in Equation 7, was used, where d is the number of parameters and $\boldsymbol{\theta}$ is the hyperparameter vector of the model to be tuned.

$$\mathrm{Cov}\left(Z\left(x^{(i)}\right), Z\left(x^{(j)}\right)\right) = \sigma^2 R\left(x^{(i)}, x^{(j)}\right) \tag{6}$$

$$R\left(x^{(i)}, x^{(j)}\right) = \exp\left(-\sum_{k=1}^{d} \theta_k \left(x_k^i - x_k^j\right)^2\right) \tag{7}$$

In each prediction, a covariance vector, $\boldsymbol{r}$, is calculated as given in Equation 8, where n_{sample} is the number of sampling points.

$$\boldsymbol{r} = \left[R\left(x, x^{(1)}\right) \quad R\left(x, x^{(\dots)}\right) \quad R\left(x, x^{(n_{sample})}\right)\right]^T \tag{8}$$

The predicted output value of new parameters is estimated by Equation 9, where y is the output vector with size $n_{sample} \times 1$, and $\boldsymbol{f}$ is the vector of ones with by the size $n_{sample} \times 1$.

$$\hat{y} = \hat{\mu} + \boldsymbol{r}_{(x)}^T \mathbf{R}^{-1}(\boldsymbol{y} - \boldsymbol{f}\hat{\mu}) \tag{9}$$

For any given $\boldsymbol{\theta}$, μ^2 and σ^2 are found using Equations 10 and 11.

$$\hat{\mu} = (\boldsymbol{f}^T \mathbf{R}^{-1} \boldsymbol{f}) \times (\boldsymbol{f}^T \mathbf{R}^{-1} \boldsymbol{y}) \tag{10}$$

$$\sigma^2 = \frac{1}{n_{sample}} (\boldsymbol{y} - \boldsymbol{f}\hat{\mu})^T \mathbf{R}^{-1} (\boldsymbol{y} - \boldsymbol{f}\hat{\mu}) \tag{11}$$

To find the best $\boldsymbol{\theta}$ vector, the maximum likelihood estimator was used, as given in Equation 12, and genetic algorithm was adopted to pick the optimal $\boldsymbol{\theta}$.

$$\max_{\boldsymbol{\theta}}\left(-\frac{n_{sample}}{2}\ln(\sigma^2)-\frac{1}{2}\ln(|\det(R)|)\right) \tag{12}$$

2.4. Ship Dynamics Model

To analyze how sailing systems affect propeller power in response to environmental conditions, a ship dynamics model, namely MMG model [16,17], was used. The equation of the motion of a ship based on the MMG model is given in Equation 13. Here, m, m_x, m_y, I_{zG}, and J_z are the mass, added mass, inertia, and added inertia terms; u and v_m are the surge and sway speeds; r is the yaw rate; x_G is the position of the center of gravity with respect to midship; X, Y, and N are the acting force and moment in the direction of surge, sway, and yaw. The subscripts H, P, R, $Sail$, and $HullWind$ indicate hull hydrodynamic forces, propeller forces, rudder forces, sail forces, and hull-wind interaction forces. Further details regarding the formulation of the model can be found in previous studies [18,19]. Target ship in the present study is KVLCC2 [20], whose length between perpendiculars is 320 m, breadth is 58 m, draft is 20.8 m, and block coefficient is 0.81.

$$\begin{aligned}(m+m_x)\dot{u}-(m+m_y)v_m r-x_G m r^2 &= X_H+X_P+X_R+X_{Sail}+X_{HullWind}\\ (m+m_y)\dot{v_m}+(m+m_x)ur+x_G m\dot{r} &= Y_H+Y_P+Y_R+Y_{Sail}+Y_{HullWind}\\ (I_{zG}+x_G^2 m+J_z)\dot{r}+x_G m(\dot{v_m}+ur) &= N_H+N_P+N_R+N_{Sail}+N_{HullWind}\end{aligned} \tag{13}$$

To evaluate the performance of sailing systems, an autopilot was integrated into the MMG model to follow a straight route at a given ship speed. Due to the interaction between the hull and the environment and forces generated by the sail, propeller revolution, and rudder angle should be controlled to ensure the same conditions exist. Thus, [illegible] comparison and evaluation are conducted.

The performance of rigid wind sails and rotor sails highly depends on their operational parameters, such as the *AoA* and spin ratio. If the interaction effect between sails is neglected, both sailing systems would have their own controller to determine [illegible] operational conditions. For example, *AoA* is determined to maximize the thrust, and spin ratio is determined to maximize the difference between the propulsive power generated by the rotor sail and the power required to rotate at operational speed. However, it is inevitable that interaction effects exist between multiple sailing systems. In this case, the optimal operational conditions would change depending on the environment. To investigate how much interaction plays a role and how an integrated controller would improve the overall performance, a case study was conducted as given in Table 3. In Case 1, the physical interaction effects are neglected, and sails are operated at their own individual optimal points. In Case 2, the physical interaction effects are included in the model, but sails operate at their own optimal points to identify how much interaction plays a role. In Case 3, the controller logic is adjusted to find the mutual optimal points, using the knowledge of the surrogate model of interaction, to measure the extent to which the integrated control approach improves the overall performance.

3. Results

First, the performance of the surrogate model developed in this study was presented in Figure 3 and Table 4. Figure 3 shows a plot with the CFD computed values on the horizontal axis and the surrogate model's predicted [illegible] values on the vertical axis, comparing the results based on each type of sail. To evaluate the errors quantitatively, the root mean square error (RMSE) and mean absolute error (MAE) were calculated as given in Table 4. In addition to RMSE and MAE values, the ratios of RMSE and MAE to the maximum value of the corresponding coefficients (RMSE/c_{max}, MAE/c_{max}) were calculated. Results indicate that the predictions made by the surrogate model are sufficiently accurate. The maximum prediction error was found to be 8.06% and 5.88% in terms of RMSE/c_{max} and MAE/c_{max} for the rotor sail's lift coefficient prediction, respectively. Therefore, it can be concluded that the surrogate model outputs have an acceptable level of accuracy.

After obtaining the surrogate model behavior, three different models corresponding to the cases given in Table 3 were created. Then, the required propeller power for each case

Table 3. *Sampling points for each input parameter*

Cases	Rotor sail control	Rigid wind sail control	Interaction effect
Case 1	*SR* to maximize net power	*AoA* to maximize sail thrust	Not included
Case 2	*SR* to maximize net power	*AoA* to maximize sail thrust	Included
Case 3	Surrogate model of interaction is integrated to maximize total net power to determine *SR* and *AoA*.		Included

SR: Spin ratio, *AoA*: Angle of attack

Table 4. *Error analysis of surrogate model*

	$C_{D,rigid}$	$C_{L,rigid}$	$C_{D,rotor}$	$C_{L,rotor}$	$C_{P,rotor}$
RMSE	0.0420	0.0921	0.1983	0.8026	0.0163
MAE	0.0347	0.0671	0.1491	0.5850	0.0123
RMSE/c_{max} (%)	3.15	6.91	6.61	8.06	1.01
MAE/c_{max} (%)	2.61	5.03	4.97	5.88	0.76

RMSE: Root mean square error, MAE: Mean absolute error was compared to the propeller power of the ship without any sailing system. As given in Figure 4, the percent propeller power reduction was calculated for the true wind speed of 10 m/s and the different true wind angles. It was found that Case 1 revealed a higher power reduction compared to other cases because the interaction effects were ignored. In the condition of true wind angles between 30 and 90 degrees, the surrogate model-informed controller in Case 3 found better operating conditions, leading to higher power reduction characteristics.

To clarify how such an integrated controlling approach achieves higher power reduction, optimal operating conditions assigned by the controller were investigated, as shown in Figure 5. Since Case 1 and Case 2 have the same controlling strategy, which neglects the interaction model, spin ratios and angles of attack were found to be almost the same. On the other hand, the integrated control approach in Case 3 leads to having different optimal spin ratios and angles of attack.

It is also important to reveal how much thrust is generated by each sailing system depending on controller type and interaction model. Figure 6 shows how much thrust is generated considering different modelling approaches based on different cases. It was found that Case 1 always overestimates the thrust generated because the interaction between sailing systems is [illegible]. Surprisingly, the integrated control action enhances the overall thrust [illegible]

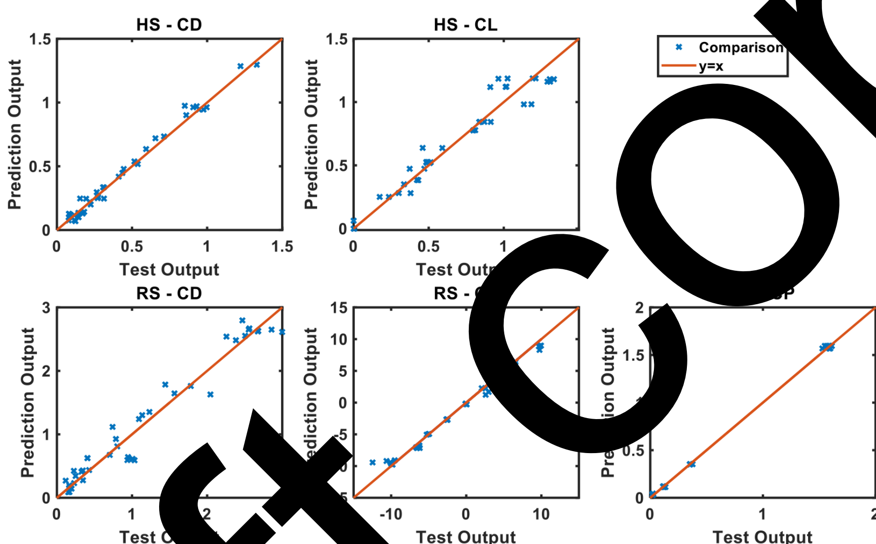

__Figure 3.__ The performance of the developed surrogate model o[illegible] C_L estimation compared to CFD-computed C_D and C_L
HS: Hard sail, CD: Drag coefficient, RS: Rotor sa[illegible]FD: Computational fluid dynamics

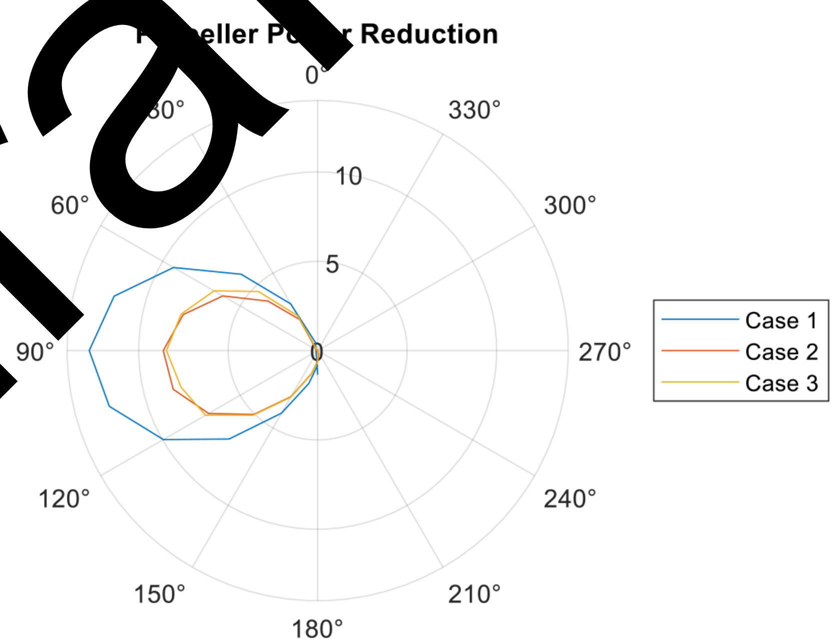

__Figure 4.__ The amount of propeller power against the wind direction in each case

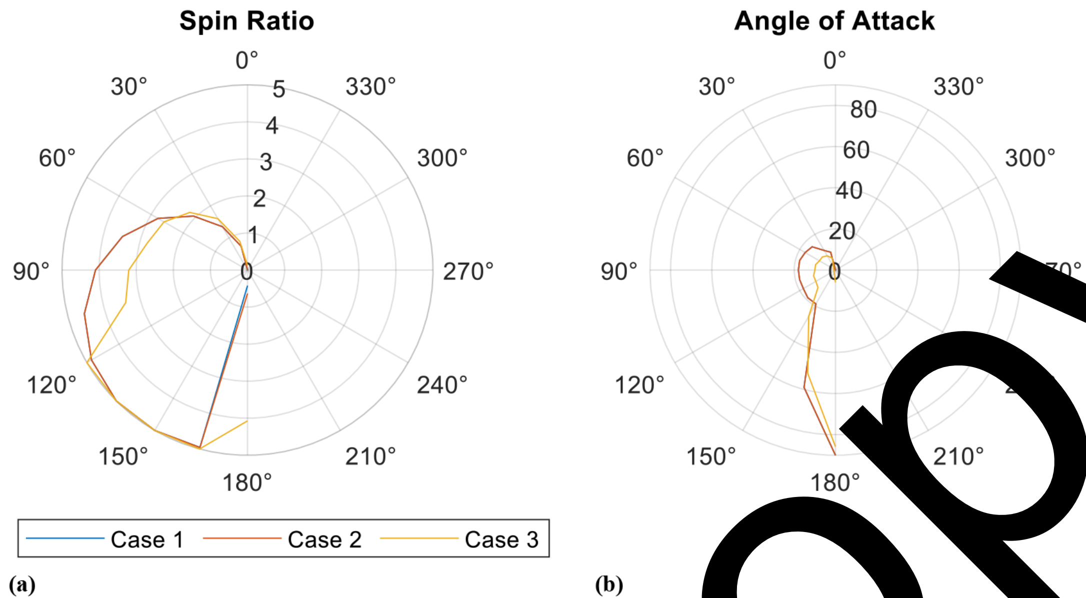

Figure 5. *The optimal* ***(a)*** *spin ratio and* ***(b)*** *angle of attack depending on the true wind direction*

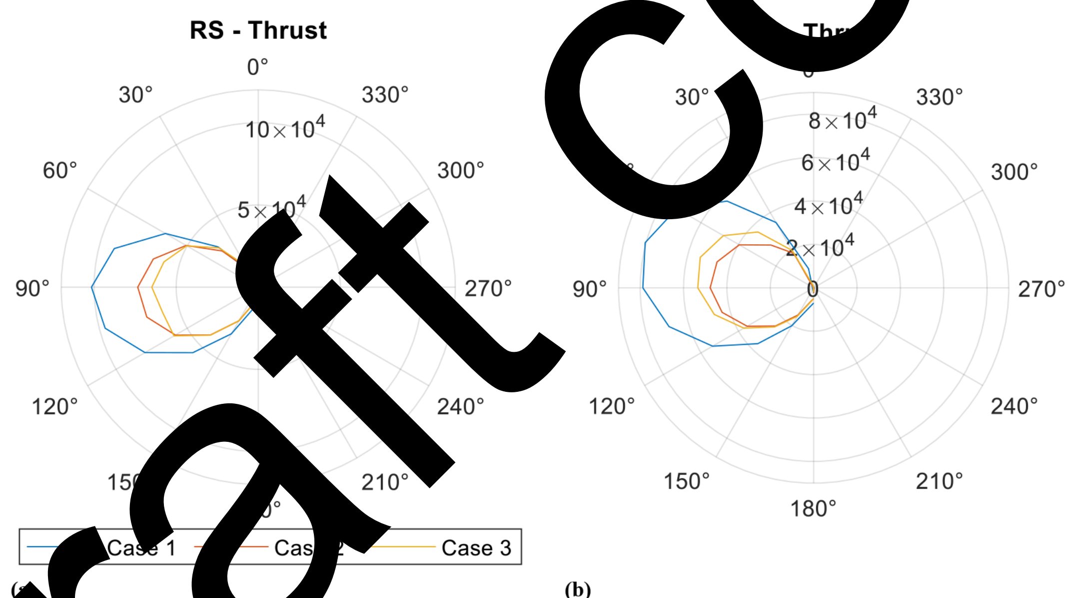

Figure 6. *The thrust generated by* ***(a)*** *rotor sail and* ***(b)*** *rigid wind sail depending on the true wind direction*

increasing the efficiency of rigid wind sail and reducing the efficiency of rotor sail.

4. Discussion

Wind-assisted propulsion systems gain attention due to their potential [illegible] fuel consumption and CO_2 emissions using wind as a free energy source. Although their implementation in vessels increases continuously, there are some challenges that need to be investigated. When wind-assist systems are integrated into ships, the additional thrust can be used without changing the operating point of the propeller. In this case, resistance will also increase as the ship speed increases. Thus, the efficiency of sailing systems drops. To avoid such a situation, propeller revolution should be controlled to maintain ship speed, thus leading to reduced propeller power and fuel consumption. In addition, the bridge, other superstructures on deck, and other sailing systems affect the actual flow speed and direction near the sail of interest. In this case, extensive CFD simulation results or experimental/operational data should be incorporated into controllers to find the optimal operating point of sailing systems. In the present study, the interaction effects of different sailing systems on the force generation characteristics of sails and the effect of CFD simulation data on the performance of sails were investigated.

The fluid interaction between the same type of sailing systems was investigated previously. Since the interaction problem is complex and dependent on many factors, some studies used simpler models, such as potential theory, to generate data. To increase the accuracy of fluid dynamics, the steady incompressible Reynolds-Averaged Navier-Stokes equations with the SST k-ω turbulence model were employed. Since the computational cost increases, a surrogate model of interaction is required. Among various methods, the kriging surrogate model with LHS was selected due to its performance with fewer sampling points. As shown in Figure 3 and Table 4, the surrogate model developed in this study demonstrates generally high prediction accuracy with a maximum 8% relative RMSE and 5.8% relative MAE. Kriging surrogate models can be considered as a suitable method to investigate the interactions of multiple sailing systems based on performance metrics, the computational cost of building a database, and requiring fewer data points. By employing such a surrogate model, the number of required simulations can be reduced significantly. On the other hand, it was observed that the performance of the surrogate model decreases when the wind direction is between 0° and 30° or 150° and 180° relative to the heading direction. This is likely due to the complex flow interactions occurring between the rigid wind sail and the rotor sail in these regions, where aerodynamic interference becomes significant. The complexity of the flow in the interaction zone is considered difficult to accurately capture using the Kriging model.

In this study, two key findings were obtained. The first is whether the aerodynamic interaction is considered or not leads to a significant difference in the resulting thrust. As shown in Figure 4 and Figure 5, Case 1, where the interaction is not considered, consistently overestimates the effect of the sails in all wind directions. Across all wind directions, Case 1 produces approximately [illegible] times more thrust than Case 2, which considers the aerodynamic interaction. When thrust generation characteristics were considered, Case 1 yields about [illegible] to 1.8 times more thrust than Case 2 across all wind directions. These results indicate that neglecting the aerodynamic interaction leads to an overestimation of thrust, suggesting that the interaction between sails has a detrimental effect on the actual thrust that can be obtained. The second key finding is that integrated control of the sails leads to better performance compared to independent operation. As shown in Figure 4 and Figure 6, Case 3—where the rigid wind sail and rotor sail are optimally operated integratively—achieves higher thrust than Case 2, where the two sails are controlled independently. In Figure 6, this advantage of integrated control is particularly evident when the wind direction is between 60° and 90°. Referring to Figure 5, which shows the *AoA* and spin ratio for the same wind directions, it can be observed that both *AoA* and spin ratio varied in Case 3. These results suggest that the integrated control strategy seeks to minimize the flow interference caused by the rotor sail, thereby allowing the rigid wind sail to generate maximum thrust. As a result, the total thrust output is effectively maximized.

In this study, the aerodynamic interaction between a rigid wind sail and a rotor sail was considered, and the thrust and energy savings achieved through integrated control were evaluated. It was confirmed that integrated operation resulted in an average reduction of [illegible]% in energy consumption across all wind directions. However, further reductions can be expected when this approach is combined with other strategies. One such strategy is route optimization, which involves adjusting the ship's sailing path to maximize wind availability. Another strategy is lowering ship speed.

5. Study Limitations

This study also has several limitations. First, the cost analysis was not conducted. For instance, operating multiple types of sails may lead to increased maintenance and operational costs. However, since the initial and running costs of rigid wind sails and rotor sails include many confidential elements, such considerations were excluded from this study. The second limitation relates to the impact on ship balance caused by the installation of sails. The addition of rigid wind sails and rotor sails may alter the center of gravity, and the rotation of the rotor sails can generate moments that may reduce the ship's stability. In actual ship operations, safety is a critical parameter, and thorough analysis will be essential for future applications.

While the multi-sail system developed in this study has demonstrated its potential to contribute to greenhouse gas reduction, it is expected that even greater performance gains can be achieved. To achieve further improvements, surrogate models that consider design parameters in addition to operational parameters may be utilized to find the optimal layouts of multiple sailing systems. Another important point is that multiple sailing systems generate significantly larger thrust and affect the operating point of the engine and propeller. To evaluate the extent of reduction in fuel consumption achieved using many sailing systems, a main engine model is required. These issues remain for future investigation and development.

6. Conclusion

In this study, we developed an integrated operational model that combines multiple types of wind-assisted devices, specifically, a rigid wind sail and a rotor sail to overcome the limitations of existing devices. For the development of the model, the aerodynamic effects arising from the operation of multiple types of sails were analyzed using CFD simulations. Based on the CFD results, a kriging surrogate model was constructed to efficiently represent aerodynamic behavior. Using the surrogate model integrated into an MMG model, researchers investigated the interaction effect and the interaction-informed controller approach. It was confirmed that when interaction model is not considered, the reduction in propeller power tends to be overestimated This discrepancy is caused by aerodynamic interference between the sails, which disturbs the flow and results in actual wind conditions deviating from the assumed input. Next, the effect of interaction-informed control was investigated. It was confirmed that integrated operation yields greater thrust and reduces fuel consumption more effectively, with particularly significant differences observed when the wind direction is between 60° and 90°. This suggests that the integrated control strategy minimizes aerodynamic interference between the sails, allowing each sail to operate as if the other were not present.

Footnotes

Authorship Contributions

Concept design: T. Endo, and C. Güzelbulut, Data Collection or Processing: T. Endo, and C. Güzelbulut, Analysis or Interpretation: T. Endo, and C. Güzelb[illegible], Literature Review: T. Endo, Writing, Reviewing [illegible] Ed[illegible]. Endo, and C. Güzelbulut.

Funding: The authors did not receive [illegible]ancial [illegible]ort for the research, authorship and/or publ[illegible] of this art[illegible]

References

[1] IMO, "Initial IMO strategy o[illegible]duct[illegible] GHG em[illegible]s from ships," [Online]. Availab[illegible] https://[illegible]o.org/en/[illegible]Work/Environment/Pages/Visio[illegible]nd-leve[illegible]-am[illegible]n-of-the-Initial-IMO-Strategy.aspx. [Acces[illegible] Jun[illegible] 2025].

[2] E. A. Bouman, E[illegible]ndstad, A. I[illegible]alland, a[illegible] A. H. Strømman, "[illegible]te-of-the-[illegible]nologies, me[illegible]es, an[illegible]otential for reducing G[illegible]missions [illegible]hipping – a re[illegible]*ransportation Research Part [illegible]ransport a[illegible]Environment*, vol. 52, Part A, pp. 408-421, 2017.

[3] [illegible]erra, and [illegible]ncello, "[illegible]ds the IMO's GHG goals: a critical [illegible]erview of the [illegible]ectives and challenges of the main options for [illegible]carbonizing inte[illegible]nal shipping," *Sustainability*, vol. 12, 3220, [illegible]0.

[4] J. [illegible]mer[illegible]S. Steen, "Sail-induced resistance on a wind-powere[illegible]ship," *Ocean Engineering*, vol. 261, 111688, Oct 2022.

[5] C. J. von Klemperer, R. A. D. Horwitz, and A. G. Malan, "An articulating wingsail design for Wind Assisted Ship Propulsion (WASP) applications," *Scientific African,* vol. 20, e01699, Jul 2023.

[6] H. Zhu, H. D. Yao, F. Thies, J. W. Ringsberg, and B. Ramne, "Propulsive performance of a rigid wingsail with crescent-shaped profiles," *Ocean Engineering*, vol. 285, 115349, Oct 2023.

[7] C. Guzelbulut, T. Badalotti, and K. Suzuki, "Optimizat[illegible]echniques for the design of crescent-shaped hard sails for wind-a[illegible]ted ship propulsion," *Ocean Engineering*, vol. 312, 119142, Nov [illegible]4.

[8] F. Tillig, and J. W. Ringsberg, "Design, [illegible]tion and an[illegible]is of wind-assisted cargo ships," *Ocean Engineer*[illegible]211, [illegible]03, Sep 2020.

[9] C. S. Kwon, S. M. Yeon, Y. [illegible]Kim, [illegible]Kim, Y. H. Kim, [illegible] H. J. Kang, "A parametric s[illegible]y for a flett[illegible]otor in standalo[illegible] condition using CFD," *I[illegible]ional Journal o[illegible]val Architectu[illegible] and Ocean Engineering,* vo[illegible] 100493, Jan 20[illegible]

[10] C. Guzelbulut, T. Badalotti, a[illegible]K. Suzuki, [illegible]mpact of control strategies f[illegible]ted sh[illegible]rgy consumption," *Brodogra*[illegible], vol. 76, 76[illegible]Nov 20[illegible]

[11] B. Goksu[illegible]d K. E. Erginer, [illegible]luation o[illegible]canopy curvature for a kite ass[illegible]d ship propulsio[illegible]ystem," *Nav[illegible]ngineers Journal,* [illegible]134, p[illegible]104, 2022.

[12] G. M. Dadd, [illegible]H[illegible], and R. A. Shenoi, "Determination of kite forces using three-dimensional flight trajectories for ship propulsion", [illegible]*ewable Energy*, vol. 36, pp. 2667-2768, Oct 2011.

[13] M. Reche-Vi[illegible]ova, et al. "Predictive surrogates for aerodynamic [illegible]rforman[illegible]nd independent sail trim optimization of multiple [illegible]ulsion system configurations," *Journal of Sailing Technology*, vol. 10, pp. 19-49, 2025.

[14] R. Zhang, et al. "A novel method of desynchronized operation of sails for ship wind-assisted propulsion system," *Ocean Engineering*, vol. 288, 115964, Nov 2023.

[15] H. Lee, Y. Jo, D. J. Lee, and S. Choi, "Surrogate model based design optimization of multiple wing sails considering flow interaction effect," *Ocean Engineering* vol. 121, pp. 422-436, Jul 2016.

[16] A. Ogawa, T. Koyama, and K. Kijima "MMG report-I, on the mathematical model of ship manoeuvring," *Bull Soc Naval Archit Jpn*, vol 575, pp. 22-28, 1977. [In Japanese]

[17] A. Ogawa, and H. Kasai, "On the mathematical method of manoeuvring motion of ships," *Int Shipbuild Prog* vol: 25(292), pp. 306–319, 1978.

[18] H. Yasukawa, Y. Yoshimura, "Introduction of MMG standard method for ship maneuvering predictions," *Journal of Marine Science and Technology,* vol. 20, pp. 37-52, 2015.

[19] C. Guzelbulut, T. Sugimoto, Y. Fujita, K. Suzuki, "Investigation of the efficiency of wind-assisted systems using model-based design approach," *Journal of Marine Science and Technology,* vol. 29, pp. 387-403,Apr 2024.

[20] MOERI KVLCC2 geometry and conditions, SIMMAN 2008, FORCE technology. [Online] http://www.simman2008.dk/KVLCC/KVLCC2/kvlcc2_geometry.html. Accessed: 27 June 2023.